Hindawi Publishing Corporation
Advances in Meteorology
Volume 2016, Article ID 6791278, 11 pages
http://dx.doi.org/10.1155/2016/6791278

Research Article

Hydrochemical Denudation and Transient Carbon Dioxide Drawdown in the Highly Glacierized, Shrinking Koxkar Basin, China

Jian Wang,[1,2] Haidong Han,[2] Qiudong Zhao,[2] and Xiaowen Zhang[3]

[1]*College of Urban and Environmental Sciences, Yancheng Teachers University, Yancheng 224002, China*
[2]*State Key Laboratory of Cryosphere Science, Cold and Arid Regions Environmental and Engineering Research Institute, Chinese Academy of Sciences, Lanzhou 730000, China*
[3]*College of Urban and Environmental Sciences, Northwest University, Xi'an 710027, China*

Correspondence should be addressed to Xiaowen Zhang; zhangsq@nwu.edu.cn

Received 18 December 2014; Revised 29 May 2015; Accepted 16 June 2015

Academic Editor: Fengjing Liu

This study considered solute fluxes and the transient CO_2 drawdown process in the highly glacierized Koxkar basin in Central Eurasia, around 70.20% of which is covered by present-day ice. From 27 June to 30 September 2011, the total runoff depth was 671.70 mm, which yielded crustal solute fluxes of 213.65 ± 10.05 kg·(km^2·d)$^{-1}$ that accounted for 53.59% of the total solute flux of the river water. The solute fluxes derived directly from ice meltwater and precipitation were 70.02 ± 4.68 and 16.57 ± 1.13 kg·(km^2·d)$^{-1}$, respectively, which accounted for 17.57% and 4.16% of the total solute flux. The carbonation and hydrolysis of carbonate and feldspar minerals occurred because of the presence of H^+, supplied by sulfide oxidation or CO_2 drawdown. While the H^+ yielded by sulfide oxidation was insufficient for hydrochemical reactions, atmospheric CO_2 dissolved in the water generated H^+ that drove follow-up reactions. The total transient drawdown of CO_2 was 804.83 t C, which generated 39.61% of the total HCO_3^- and 24.68% of the river water solute. Transient drawdown of CO_2 in the glacier region indicated that change of glacial area and volume could influence atmospheric CO_2 concentration and be important in the long-term global CO_2 cycle.

1. Introduction

From 1880 to 2012, the global mean surface air temperature has increased by 0.85°C and this increase has been especially pronounced since about 1950 [1]. For example, in the extensively glaciated Tarim basin in China, the mean surface air temperature has increased by 0.6°C since the 1980s (i.e., 0.2°C per decade). This rate of warming has had considerable influence on the alpine glaciers and hydrology of such regions. Overall, 82.2% of glaciers have retreated and the total glacial area has reduced by 4.5% [2]. Furthermore, because of climate warming resulting from increased greenhouse gas forcing, the volume of glacial meltwater has increased by about 1.24×10^8 m^3·a^{-1}, which accounts for about 15% of the increase in river discharge in the Tarim basin [3]. Increased river discharge increases crustal solute fluxes (or chemical denudation rates) and CO_2 drawdown rates [4, 5] because of hydrochemical reactions.

A few studies have reported on chemical denudation rates and CO_2 drawdown rates in the glaciers of the Arctic, Alps, and Himalayan mountains [4, 6–13]. These reports suggested that denudation rates in glaciated areas were higher than in nonglaciated regions [7]. In Central Asia, there are many large glaciers (area > 50 km^2) covered by supraglacial moraines. Because they are in regions far from the ocean, there is little precipitation and ice/snow meltwater has particular importance as a water resource. However, a review of chemical denudation rates is beyond the scope of the present paper.

The focus of the present study was to examine the fluxes of major ions emanating from a subglacial outlet, to assess the rate of chemical denudation and sequestration of

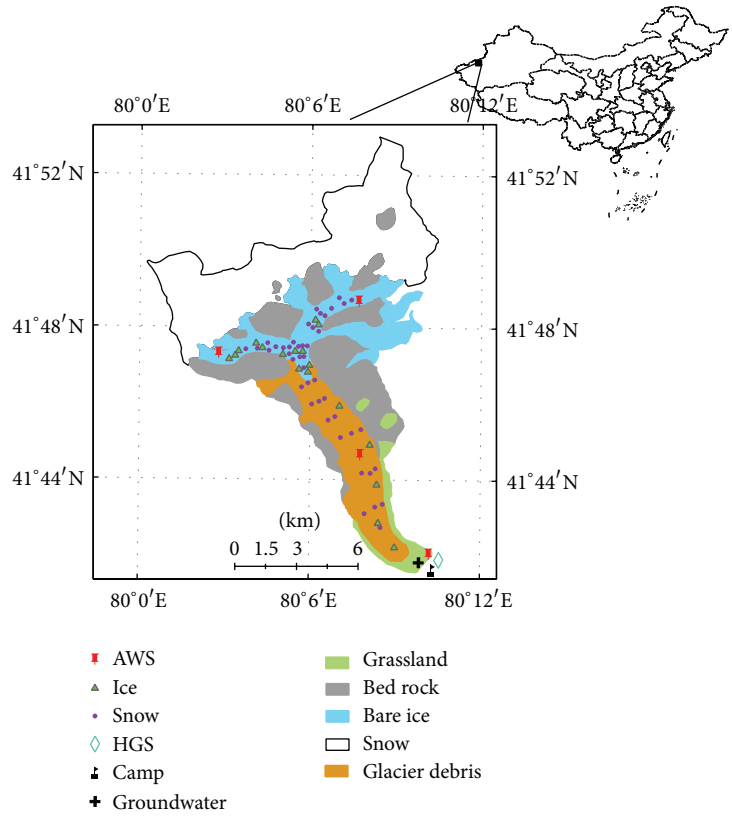

Figure 1: Location of study area and positions of sampling sites in the Koxkar glacier region.

atmospheric CO_2 in the glacierized Koxkar basin in Central Asia, based on major ion concentrations in the water. The results provide new data on ion concentrations in large alpine glacierized basins covered by supraglacial moraines, which could be used for modeling and the estimation of CO_2 changes during the last glacial maximum.

2. Study Area

2.1. Site Description. The Koxkar basin is located on the southern side of Mt. Toumuer in Northwest China (41°47′N, 80°04′E). The watershed covers an area of 118.12 km^2, of which around 70.20% is covered by present-day ice (Figure 1). There are systems of deep meltwater shafts (moulins) above 3900 m a.s.l. The glacier has a subcontinental regime with subglacial outflow issuing from a conduit at the center of the glacier snout.

The mean annual air temperature observed near the glacier terminus is 0.77°C, and the mean summer (May–September) temperature is 7.74°C [14]. The monthly mean air temperature is >0°C for about 6 months. The main source of precipitation is water vapor derived from the Atlantic and Arctic oceans [15]. The annual average precipitation is about 630.3 mm at the glacier terminus, 81.24% of which occurs in summer. Precipitation in the glacierized region is mainly solid state (snow or hail).

A field investigation during 2003–2012 suggested that the discharge at the hydrological gauging station (HGS) at the glacial terminus was $>1.0 \times 10^8$ $m^3 \cdot a^{-1}$ (Figure 1) and that the runoff flux from May to October accounted for ~94.5% of the annual total [14].

2.2. Geological Setting. Terranes from the Precambrian to Quaternary are exposed in the valleys of the Koxkar basin. Marine terrigenous clastic rocks and carbonates are very important to the regional geology, but their depths are unknown. There is little territorial volcanism [16]. Biotite monzogranite gneiss and augen granite gneiss are exposed above 3900 m a.s.l. in the Koxkar basin. From 3900 to 3400 m a.s.l., marble, shale, and rocks, which enrich the tremolite and biotite of the parametamorphic rock, are distributed on two hillsides, and marine sediment shale is exposed from 3300 to 3400 m a.s.l., supplying large quantities of substances that are important to the carbonation and oxidation processes in the subglacial environment. In other regions of the Koxkar basin, there are tertiary mudstones, siltstones, and glutenite distributed in supraglacial and terminal moraines. The area of the superglacial moraine accounts for ~83% of the total melting area [17].

3. Methods

Four automatic weather stations (AWSs) were established in 2007 (Figure 1). Hourly air temperature, precipitation, wind direction and velocity, and radiation were measured and recorded by the AWS positioned near the camp, while

the other AWSs mainly measured precipitation, air temperature, humidity, and wind speed.

Since 28 June 2011, river water sampling has been conducted at the HGS 200 m downstream of the main subglacial outlet. This sampling site was chosen because of inaccessibility near the subglacial outlet and to avoid sampling before the different water masses were thoroughly mixed [9]. During the sampling period, bulk meltwater samples were taken manually at around 14:00 Beijing time (BT) daily (96 in total). This sampling time was chosen because the specific conductivity (SpC) at 14:00 BT represents 96.72% of the mean of the hourly samples taken during the first 10 days. Additionally, 18 ice samples and 42 precipitation (snow) samples from the ablating area of the Koxkar glacier were collected along the direction of glacial development between 2996 and 4026 m a.s.l. (Figure 1). Furthermore, 9 groundwater samples from a spring located south of the main river bed and 16 rainfall samples from the observation camp were collected.

All samples were collected manually in prerinsed polypropylene bottles containing as little air as possible. Bottles and lids were rinsed in the sampling water before collection and disposable gloves were used to avoid contamination. The ice samples from the ablating region were collected after melting in a disposable polypropylene bag. At the camp, all samples were stored in a dark and cold location. Bottled samples, which were in a frozen state in insulated boxes, were transported to the State Key Laboratory of Cryosphere Science—of the Cold and Arid Regions Environmental and Engineering Research Institute, Chinese Academy of Sciences—and kept in a cold room at −20°C. Three blank samples were assessed to ensure that the cumulative contamination was below the baseline for each measured chemical species. After the samples were retrieved, they were immediately analyzed for pH and SpC using a pH meter (PHSJ-4A; measurement range of 0–14, uncertainty within ±0.005) and a conductivity meter (DDSJ-308A; measurement range of 0–999 $\mu s \cdot cm^{-1}$ and uncertainty of less than 5‰), respectively. Then, the precipitation, bulk meltwater, groundwater, and ice meltwater samples were gradually warmed to a temperature of 20°C.

Major cations (Na^+, K^+, Mg^{2+}, and Ca^{2+}) were analyzed using a Dionex ISC 600 ion chromatograph with 20 mM MSA (methanesulfonic acid) eluent and CSRS suppresser (uncertainty <0.1%). Major anions (Cl^-, NO_3^-, and SO_4^{2-}) were analyzed using a Dionex ISC 300 ion chromatograph with 25 mM KOH eluent and ASRS suppresser (measurement range of 0.5–400 μm, uncertainty <0.5%) [6]. The water samples were analyzed for $\delta^{18}O$ values using the CO_2 equilibration method with a gas bench, which was interfaced with a MAT-252 isotope ratio mass spectrometer. The $^{18}O/^{16}O$ ratio was expressed as the difference in parts per thousand relative to the Vienna Standard Mean Ocean Water. The precision of the $\delta^{18}O$ measurement was 0.2%.

Notably, the summations of the contents of major cationic (Na^+, K^+, Mg^{2+}, and Ca^{2+}) and anionic (F^-, Cl^-, SO_4^{2-}, and NO_3^-) electronic charges appeared unbalanced. Ratios of ∑(cations)/t(anions) for bulk river water, precipitation, groundwater, and glacial ice meltwater were 3.49, 3.07, 3.92, and 2.81, respectively, implying that there was at least one anion present that was not considered in the experiment. The mean pH of 8.12 and the maximum value of only 8.70 indicated that CO_3^{2-} was not present in the different waters from the study area. Therefore, we determined the HCO_3^- concentration from ionic charge balances [8, 12, 18, 19], that is, the sum of all cationic charges ($\sum^+$) minus the sum of all anionic charges ($\sum^-$):

$$\text{Charge}\left(HCO_3^-\right) = \sum^{+} - \sum^{-}. \quad (1)$$

To verify the reliability of the HCO_3^- calculation in (1), the 13 river water samples were analyzed using the titrimetric method. The average error was 2.30% and the maximum margin of absolute error was 7.40×10^{-5} mol·L^{-1}. Unfortunately, most of the sample volumes were not large enough to be measured using the titrimetric method and ultimately, the titrimetric method was not considered because of atmospheric CO_2 contamination to the HCO_3^- at the time of sample collection.

4. Results

4.1. Meteorology and Hydrology. From 27 June to 30 September 2011, the mean daily air temperature was 9.8°C. The highest temperature recorded was 16.1°C on 6 August and the lowest temperature was 2.0°C on 17 September (Figure 2(a)). Contemporaneous, total precipitation was 260.8 mm, which was mostly solid state (i.e., snow, hail, or sleet). The largest precipitation total was 28.0 mm on 12 August (Figure 2(b)).

The minimum and maximum daily discharges at the HGS were 2.94 and 17.00 $m^3 \cdot s^{-1}$, respectively, and the mean daily discharge was 9.57 $m^3 \cdot s^{-1}$. The total discharge volume was 7.93×10^7 m^3 (Figure 2(c)). The daily runoff obviously changed with the mean daily temperature, but it showed a clear hysteretic characteristic.

4.2. Hydrochemistry. The mean SpC of the meltwater throughout the entire observation period was 177.98 $\mu s \cdot cm^{-1}$ (range 110.00–284.00 $\mu s \cdot cm^{-1}$), which is higher than that reported (95.13 $\mu s \cdot cm^{-1}$) in 2003 (Table 1) [20]. It is also higher than the electrical conductivities recorded in both the headwaters of the Гrümuqi River (118.57 $\mu s \cdot cm^{-1}$) [21] and the meltwater of the Kartamak glacier area in Muztag Ata (85.50 $\mu s \cdot cm^{-1}$) in Northwest China [22]. However, rainfall, especially continuous rainfall, probably led to lower air temperatures and this would lead to a reduction in the melting of ice. There was an opposite relation between the intensity of the chemical reaction of the water-rock interface and the water flow speed; hence, lower water flow speed indirectly increased the SpC of the river water on a cloudy day.

The mean SpC of the glacial ice (mean 21.73 $\mu s \cdot cm^{-1}$, range 8.11–34.10 $\mu s \cdot cm^{-1}$) was lower than the mean SpC of the precipitation (mean 30.16 $\mu s \cdot cm^{-1}$, range 6.33–151.8 $\mu s \cdot cm^{-1}$) in the Koxkar basin. Generally, the SpC of glacial ice should

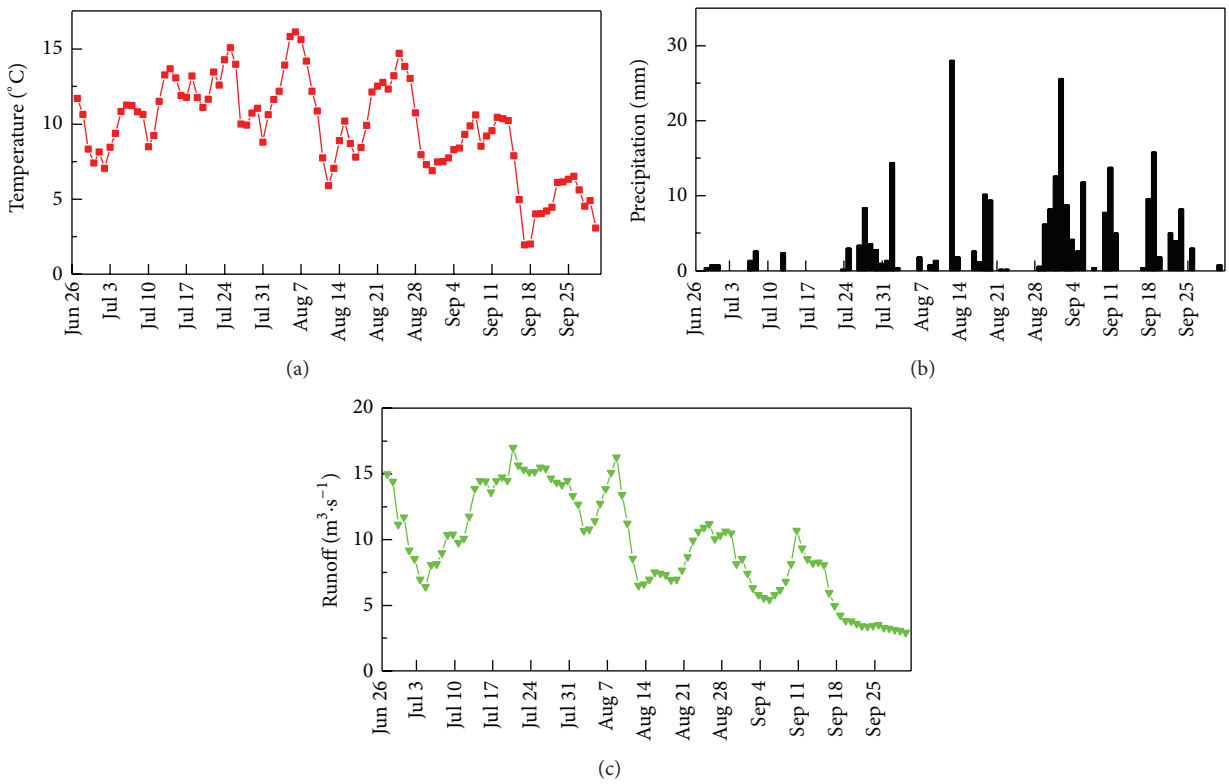

FIGURE 2: Daily average (a) air temperature, (b) precipitation, and (c) discharge in the Koxkar region from 27 June 2011 to 30 September 2011.

TABLE 1: Differences in ion concentrations of different waters in the Koxkar basin ($\times 10^{-6}$ mol·L^{-1}).

Item	N[1]	Na^+			K^+			Mg^{2+}			Ca^{2+}		
		Mean	Max	Min	Mean	Max	Min	Mean	Max	Min	Mean	Max	Min
Glacial ice	21	9.23	29.00	1.78	1.93	6.92	0.26	12.19	33.92	1.83	63.90	108.25	25.25
Precipitation	58	25.29	226.90	1.44	2.71	10.57	0.15	13.86	55.01	0.31	63.01	148.03	2.50
Groundwater	9	353.85	372.74	332.56	111.44	115.35	108.24	269.95	301.20	233.17	240.99	297.72	172.33
River water	96	139.00	403.20	27.51	50.27	121.87	11.04	76.64	170.33	10.19	210.33	436.50	72.44
Item	N	F^-			Cl^-			SO_4^{2-}			NO_3^-		
		Mean	Max	Min	Mean	Max	Min	Mean	Max	Min	Mean	Max	Min
Glacial ice	21	1.72	4.32	0.48	3.92	11.69	0.93	3.91	10.73	0.56	—	—	—
Precipitation	58	0.86	2.22	0.23	19.07	117.07	1.29	11.26	37.00	1.69	3.44	18.95	1.04
Groundwater	9	25.69	28.74	23.10	96.41	110.53	75.40	120.49	188.52	95.80	14.52	17.21	11.25
River water	96	15.80	26.89	4.32	34.48	61.55	6.19	80.08	146.71	11.44	9.24	16.50	16.50
Item	N	HCO_3^-			$\delta^{18}O$			SpC			pH		
		Mean	Max	Min	Mean	Max	Min	Mean	Max	Min	Mean	Max	Min
Glacial ice	21	149.89	284.55	54.82	−10.73	−9.63	−11.99	21.73	34.10	8.11	8.07	8.96	7.02
Precipitation	58	136.38	389.66	0.00	−9.97	−0.55	−18.75	30.16	151.80	6.33	6.88	8.12	6.31
Groundwater	9	1109.59	1290.12	903.10	−11.04	−10.36	−11.01	225.80	274.00	204.00	8.16	8.40	7.86
River water	96	543.53	1107.85	126.49	−10.50	−9.59	−11.38	177.98	284.00	110.00	8.13	8.70	7.55

[1] N is the number of samples.

be higher than that of precipitation because of soluble material exchange during the formation of the ice. However, the difference here is probably because the ice samples reflected the accumulated historical precipitation in the Koxkar basin. The average SpC of the water samples decreased in the following order: groundwater > river water > precipitation > glacial ice.

The river water was alkaline (pH 7.55–8.70). The order of $\delta^{18}O$ of the different water samples was as follows: precipitation > river water > glacial ice > groundwater

(Table 1). It is important to note that an average value of $\delta^{18}O$ for groundwater was adopted when calculating the volumes of different waters in the river discharge because systematic groundwater sampling had not been performed. Concentrations of NO_3^- in some samples (especially ice meltwater) are probably lower than the lower limit of the Dionex ISC 300 ion chromatograph. Thereby, the anionic concentrations of both groundwater and river water were in the following order: $HCO_3^- > SO_4^{2-} > Cl^- > F^- > NO_3^-$, whereas precipitation had the following order: $HCO_3^- > Cl^- > SO_4^{2-} > NO_3^- > F^-$, and ice had the following order: $HCO_3^- > Cl^- > SO_4^{2-} > F^- > NO_3^-$ (Table 1). The HCO_3^- of the different types of water played a predominant role and accounted for 94.01%, 81.19%, 79.57%, and 79.75% of the anion concentrations of ice meltwater, groundwater, river water, and precipitation, respectively. The reason for this phenomenon was carbonation with river water and groundwater because of widespread marble, shale, and marine sediment shale [16]. The HCO_3^- of precipitation and ice meltwater mainly originated from regional Asian dust [23].

The order of the cationic concentrations of glacial ice ($Ca^{2+} > Mg^{2+} > Na^+ > K^+$) differed from that of river water and precipitation ($Ca^{2+} > Na^+ > Mg^{2+} > K^+$). The specific reasons for this are as follows. First, there was an interchange of material between raindrops and aerosols during ice formation after the precipitation reached the surface [24–26]. Second, the dry/wet sedimentation of atmospheric dust affected the chemical composition of river water and ice meltwater [24–27]. Third, the ice samples were collected from the area of glacial ablation and thus they were related to historical precipitation/snow. Fourth, sulfide oxidation and carbonate hydrolysis affected the river water composition, which made it distinguishable from the ice composition [6–8, 11]. In addition, the higher Ca^{2+} and lower K^+ concentrations of the different water samples were consistent with the geochemical composition of the marine deposit [28]; this also reflected the function of the regional geological setting. The transformation of $Mg^{2+} > Na^+$ of the glacial ice into $Na^+ > Mg^{2+}$ of the river water was controlled largely by the hydrochemical denudation rate and the chemical composition of the groundwater and precipitation in the Koxkar glacier basin [11, 24].

5. Discussion

5.1. Water Origin

5.1.1. Oxygen Isotope Provenance Model. Hydrograph separation of bulk meltwater has been described in attempts to quantify the recharge of different water sources [29–32]. The $\delta^{18}O$ has been chosen as one indicator. First, seasonal variations in the development of the inner drainage system of the glacier influence the residence time of water within the glacial area and thus cause variations in the chemical composition of the water sources [33, 34]. Second, the ion species used are not conservative and are exposed to chemical reactions after the components have mixed.

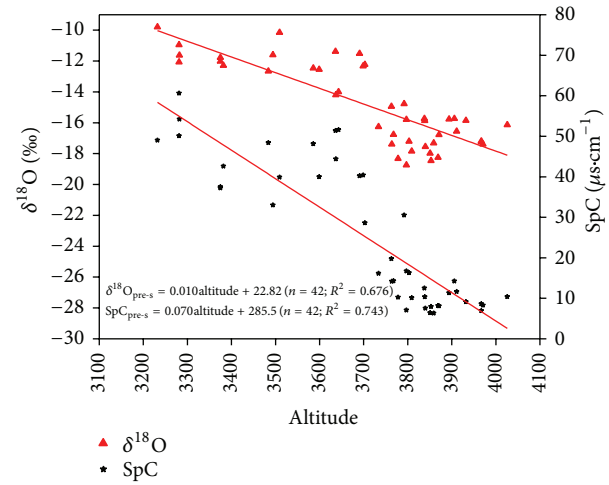

Figure 3: Relationship between $\delta^{18}O$ and SpC of spatial precipitation and altitude in melting area of the Koxkar glacier.

Although some degree of isotopic fractionation can be expected at the water-ice and water-air interfaces in the drainage system, stable isotopes are assumed more conservative than major ions [35, 36]. The water flow and oxygen isotopes issuing through the hydrographic section of the Koxkar River at any specific time can be divided into three provenances as follows:

$$\begin{aligned} Q_{\text{bulk}} &= Q_{\text{ice}} + Q_{\text{pre}} + Q_{\text{ground}}, \\ Q_{\text{bulk}}\delta_{\text{bulk}} &= Q_{\text{ice}}\delta_{\text{ice}} + Q_{\text{pre}}\delta_{\text{pre}} + Q_{\text{ground}}\delta_{\text{ground}}, \end{aligned} \tag{2}$$

where Q is discharge, δ is the $\delta^{18}O$ value, and the subscripts denote river water (bulk), ice meltwater (ice), precipitation (pre: including liquid water, snow, and hailstone), and underground water (ground).

The hydrograph separation was performed using the $\delta^{18}O$ value of each precipitation event. The $\delta^{18}O$ value of precipitation varied on both spatial and temporal scales and in addition, its dependence on altitude was considered. The relationship between altitude and the $\delta^{18}O$ value of precipitation (snow) was established (Figure 3):

$$\delta^{18}O_{\text{pre-}s\text{-}i} = 0.01 * \text{Altitude}_i + 22.82. \tag{3}$$

Actually, precipitation was extremely spatially inhomogeneous; it decreased by 7.00% from 3000 to 3700 m a.s.l. and increased by 46.60% from 3700 to 4200 m a.s.l. in the Koxkar basin [14]. Considering the dependence of precipitation volume on altitude, the following equation was derived for the corrected value of $\delta^{18}O$ of precipitation in the ablating region:

$$\delta^{18}O_{c\text{-pre}} = \sum \frac{\delta^{18}O_{\text{pre-}s\text{-}i} * P_i A_i}{\sum (P_i A_i)}, \tag{4}$$

where $\delta^{18}O_{\text{pre-}s\text{-}i}$ is the $\delta^{18}O$ value of precipitation at altitude i (m), $\delta^{18}O_{c\text{-pre}}$ is corrected $\delta^{18}O$ value of precipitation in

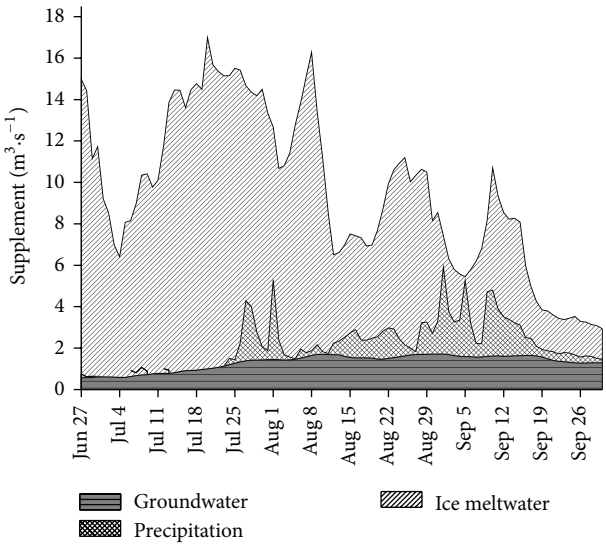

Figure 4: Supplement of precipitation, groundwater, and ice meltwater to river water in the Koxkar glacier region.

the melting area, and P_i and A_i are the total precipitation and the area, respectively, at altitude i.

To determine the relative amounts of supply of the three provenances, another indicator is required to solve the equation set. The relationship between the $\delta^{18}O$, SpC, and all soluble ionic concentrations of the river water was tested. The relationship between the $\delta^{18}O$ and SpC was poor ($R = -0.118$), which indicated that SpC was an independent parameter that could be used as one indicator to separate the river water [37–39]. The SpC of precipitation, which was referred to during the calculation, was similarly corrected as the precipitation $\delta^{18}O$.

5.1.2. Hydrological Separation. The results of the hydrograph separation using $\delta^{18}O$ and SpC suggested that glacial ice meltwater dominated the streamflow, accounting for 76.49 ± 4.58% of the total discharge from 27 June to 30 September 2011. This was followed by groundwater, which accounted for 13.71 ± 3.06% of the total discharges. The least influential was precipitation, which accounted for 9.79 ± 1.64% of the total discharge (Figure 4). The ratio of ice meltwater supplied to river runoff was 80%, as calculated by applying a degree-day model from Zhang et al. [40], which suggested that the result of the hydrological separation was reliable.

5.2. Hydrochemical Erosion

5.2.1. Solute Provenance during Erosion. The results of empirical orthogonal functions (EOFs) might be accepted for soluble ions of river water in Koxkar basin [23] (Table 2). Four feature vectors accounted for 94.2% of the cumulative variance. EOF1 which was strongly related to Na^+, K^+, Mg^{2+}, Cl^-, SO_4^{2-}, and HCO_3^- describes the main ion yield variance and accounted for 35.7% of the total ionic variance. In general, sources and quantities of Na^+ and Cl^- are connected with the

Table 2: Joint empirical orthogonal function analysis of the major ion concentrations of the river samples collected in the Koxkar basin.

Item	EOF1	EOF2	EOF3	EOF4
Na^+	0.811	−0.560	−0.273	0.073
K^+	0.829	−0.535	−0.215	0.087
Mg^{2+}	0.832	−0.541	−0.114	0.108
Ca^{2+}	0.676	0.024	0.722	−0.129
F^-	0.574	0.655	0.188	0.407
Cl^-	0.833	0.615	−0.258	−0.142
SO_4^{2-}	0.850	0.582	−0.086	0.096
NO_3^-	0.795	0.418	−0.155	−0.672
HCO_3^-	0.775	−0.486	0.599	0.046
Total variance explained (%)	35.67	26.02	17.66	14.81

transport intension of marine aerosols. However, the Koxkar basin is in Central Eurasia and is far from any sea or ocean. Fan [41] reported that bedrock in the Koxkar basin is chiefly Mesozoic sedimentary rock and metasediment with flesh-red alkali-feldspar granite intruding into off-white monzonitic granite. Thus, Na^+ and K^+ are likely provided by chemical erosion during the runoff of precipitation and snow/ice meltwater. The main reactions are represented by

$$K(AlSi_3O_8) + H^+ \longrightarrow H(AlSi_3O_8) + K^+ \quad (5)$$

$$Na(AlSi_3O_8) + H^+ \longrightarrow H(AlSi_3O_8) + Na^+ \quad (6)$$

Although there was little olivine or pyroxene, the marine clastic rocks and carbonates of the Paleozoic era were massively distributed along the upper lateral ridge and in debris of the Koxkar glacier region. However, these were not only an important Mg^{2+} source but also sources of Cl^- and Na^+ [42–44]. Therefore, EOF1 mainly represents the hydrolysis of the feldspar and carbonate of the metamorphic rock, which supplies soluble matter to the river water.

EOF2 accounted for 26.0% of the total ion variance and it related greatly to F^-, Cl^-, and SO_4^{2-} and partially to Na^+ and K^+. The ratio of $[Na^+ + K^+]/[F^- + Cl^- + 2SO_4^{2-}]$ was 0.94, which implies that hydrochemical exchange reactions existed. There was some pyrite (FeS_2) in the debris on the glacier surface and a coal seam on the glacial lateral ridge, which probably supplied abundant material for the oxidation of sulfides:

$$4FeS_2 + 15O_2 + 8H_2O \longrightarrow 2Fe_2O_3 + 16H^+ + 8SO_4^{2-} \quad (7)$$

This reaction yields H^+, which promotes the hydrolysis of K/Na-feldspar and sedimentary rock minerals and increases Na^+, K^+, and Cl^- concentrations. Therefore, EOF2 represents chemical erosion involving the sulfide oxidation of acidic materials. However, the ratio of $[Na^+ + K^+]/[F^- + Cl^- + 2SO_4^{2-}]$ was $0.94 < 1.00$, which also suggested that there might be another chemical reaction.

EOF3 accounted for 17.7% of the total ion variance relating to Ca^{2+} and HCO_3^- in the glacial runoff, which suggests that

Table 3: Solute provenances and amounts of chemical denudation in the Koxkar region [kg·(km^2·d)$^{-1}$].

Item	Na^+	K^+	Mg^{2+}	Ca^{2+}	F^-	Cl^-	SO_4^{2-}	NO_3^-	HCO_3^-
Chemical denudation	18.89	12.46	9.80	42.94	1.94	7.05	48.46	3.56	166.94
Ice meltwater	1.16	0.41	1.60	13.95	0.18	0.76	2.05	0.01	49.91
Precipitation	0.91	0.25	0.37	2.78	0.04	0.62	1.49	0.43	9.69
Solute of river water	20.96	13.13	11.77	59.68	2.16	8.42	52.00	4.00	226.54

the sources were alike, that is, calcium salt carbonation, as described by

$$CaCO_3 + CO_2 + H_2O \longleftrightarrow Ca^{2+} + 2HCO_3^- \quad (8)$$

The ratio of $[Ca^{2+}]/[HCO_3^-]$ was 0.80 > 0.50; therefore, the H^+ of carbonation was beyond that of atmospheric CO_2 drawdown. Furthermore, this also explained why the ratio of $[Na^+ + K^+]/[F^- + Cl^- + 2SO_4^{2-}]$ was <1.00.

EOF4 described 14.8% of the total ion variance, relating mostly to NO_3^-. However, the NO_3^- concentration for river water only accounted for 0.82% of the total ion concentration in the Koxkar basin. The NO_3^- concentration is the main factor governing the abundance of subglacial anaerobes, and it is affected by human activities such as industry, agriculture, and the herding of cattle and sheep [45]. Because nitrate in the natural world is present as an easily soluble salt, it is nearly impossible for it to be in the form of a solid in a glacierized basin. Hence, the NO_3^- in river water was likely due to the presence of aerosols in dry/wet deposition and material exchange at the atmosphere-hydrosphere interface during precipitation events and the formation of runoff.

5.2.2. Evaluation of Hydrochemical Denudation Rates. The crustal component of chemical denudation rates (CDRs) is equal to the total solute flux of river water minus the solute fluxes of precipitation, ice meltwater, dry/wet sedimentation of atmospheric dust, and exchange at the gas-liquid interface (see (9)). As little of the crustal component was supplied by dry/wet sedimentation of atmospheric dust and exchange at the air-liquid interface, these processes can be ignored in the analysis of basin erosion [46–48]. Table 3 presents the results according to ionic equilibrium. From 27 June to 30 September 2011, the total solute flux of chemical erosion was 312.05 ± 17.42 kg·(km^2·d)$^{-1}$ (3.54 ± 0.22 × 10^6 kg gross) (Table 3), which implies that chemical erosion for a continental glacier in the Koxkar glacier region is more intense than for some oceanic glaciers [4, 9, 49] and nonglacier regions [50–52]. In contrast, HCO_3^- erosion was strongest with a flux of 166.94 ± 9.31 kg·(km^2·d)$^{-1}$. The second strongest fluxes were the erosions of sulfide oxidation (SO_4^{2-}) and Ca^{2+} with values of 48.46 ± 2.70 and 42.94 ± 2.16 kg·(km^2·d)$^{-1}$, respectively. The erosions of Na^+, K^+, Mg^{2+}, Cl^-, and NO_3^- were weaker with fluxes of 18.89 ± 1.05, 12.46 ± 0.69, 9.80 ± 0.55, 7.05 ± 0.39, and 3.56 ± 0.47 kg·(km^2·d)$^{-1}$, respectively. The F^- erosion was the least intense with a flux of only 1.94 ± 0.26 kg·(km^2·d)$^{-1}$. In total, the solute fluxes of river water supplied by precipitation and ice meltwater were only 16.57 ± 1.13 and 70.02 ± 4.68 kg·(km^2·d)$^{-1}$, respectively, accounting for 4.16% and 17.57% of the total flux. The CDR accounted for 78.28% of the total flux:

$$\mathrm{CDR} = 3600 * 24 * 10^{-6} * \frac{\left(Q_{\mathrm{bulk}} * C_{\mathrm{bulk}\text{-}j} - Q_{\mathrm{pre}} * C_{\mathrm{pre}\text{-}j} - Q_{\mathrm{ice}} * C_{\mathrm{ice}\text{-}j} - D\right)}{\left(A * I_j\right)}, \quad (9)$$

where CDR is the crustal component of the CDRs [kg·(km^2·d)$^{-1}$]; Q_{bulk}, Q_{pre}, and Q_{ice} are the bulk river water, precipitation, and ice meltwater supplements, respectively (m^3·S^{-1}); C_{bulk}, C_{pre}, and C_{ice} are the ion concentrations of river water, precipitation, and ice meltwater, respectively (×10^{-6} mol·L^{-1}); I is molecular weight; j represents the ion species; and D is the dry/wet sedimentation of atmospheric dust, which was ignored.

5.3. Carbon Dioxide Drawdown during the Ablation Period

5.3.1. Sulfide Provenance. The reason for considering sulfide provenance is because, in nature, most reactions of chemical denudation need abundant H^+, the provenance of which is not limited to transient CO_2 drawdown (8) but includes sulfide oxidation processes (7). Thus, when calculating H^+ processes, crustal sulfate ($^{\mathrm{cru}}SO_4^{2-}$) flux is equal to the total sulfate flux minus the sulfate flux of precipitation and ice meltwater:

$$^{\mathrm{cru}}SO_4^{2-} = {}^{\mathrm{tot}}SO_4^{2-} - {}^{\mathrm{pre}}SO_4^{2-} - {}^{\mathrm{ice}}SO_4^{2-} \quad (10)$$

The SO_4^{2-} fluxes of river water (total), precipitation, ice meltwater, and crustal chemical erosion are depicted in Figure 5. The total SO_4^{2-} flux of river water was ~52.00 ± 2.47 kg·(km^2·d)$^{-1}$ and crustal chemical erosion accounted for about 93.21% of the total SO_4^{2-} flux. The second largest contribution was that supplied by ice melting, which accounted for ~3.94%. The mean SO_4^{2-} recharge attributed to precipitation was ~1.49 ± 0.88 kg·(km^2·d)$^{-1}$, which accounted for only ~2.86% of the total flux. As with SpC, the SO_4^{2-} flux of river water also decreased with increasing precipitation in the Koxkar basin, as observed on 1 and 12 August 2011 (Figure 5).

5.3.2. CO_2 Drawdown. There is considerable Paleozoicmarine terrigenous clastic rock, carbonatite, and Quaternary moraine debris in the Koxkar basin, and the amount of crustal bicarbonate (HCO_3^-) released during hydrochemical erosion mainly depended on the carbonation of carbonate and aluminosilicate (silicate). The second largest source was the hydrolysis of limestone and dolomite, induced by the oxidation of sulfides. As the Koxkar basin is in Central Eurasia

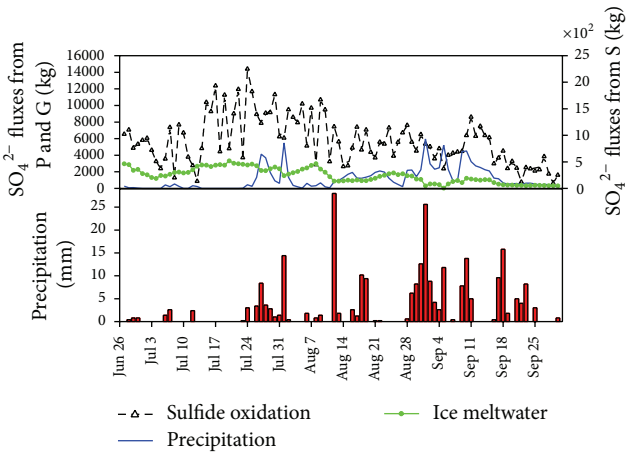

FIGURE 5: SO_4^{2-} daily fluxes for different sources and river water in the Koxkar region from 27 June to 30 September 2011 (P: precipitation; G: ice meltwater; S: sulfide oxidation).

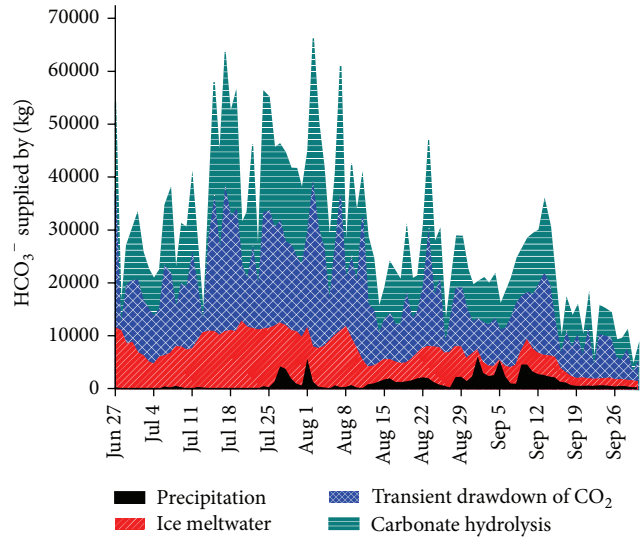

FIGURE 6: Daily flux of HCO_3^- originating from precipitation, ice meltwater, carbonate hydrolysis, and transient drawdown of CO_2 in the Koxkar region during the sampling period.

and is largely unaffected by human activity, the main supply of SO_4^{2-} was the oxidation of pyrite [11, 53]. This process yields H^+, as seen in (7). This provision of H^+ accelerates the hydrolysis of highly charged ions, such as Mg^{2+} and Ca^{2+}:

$$4FeS_2 + 15O_2 + 8H_2O + 16CaCO_3 \longrightarrow 2Fe_2O_3 + 16Ca^{2+} + 8SO_4^{2-} + 16HCO_3^- \quad (11)$$

The case for Mg^{2+} is similar. The total mass of crustal Ca^{2+} and Mg^{2+} was $1.68 \pm 0.31 \times 10^7$ mol, which is more than twice the $^{cru}SO_4^{2-}$ mass of $0.57 \pm 0.07 \times 10^7$ mol in the Koxkar basin. This implies that some of the Mg^{2+} and Ca^{2+} yield is due to atmospheric CO_2 drawdown, according to (8). Hence, the amounts of $^{pyrite}Mg^{2+}$ and $^{pyrite}Ca^{2+}$ yielded by the oxidation of pyrite and calculated by (11) should be equal to twice the amount of $^{cru}SO_4^{2-}$ [53].

The mass of Ca^{2+} and Mg^{2+} in the chemical erosion due to carbonate hydrolysis resulting from atmospheric CO_2 drawdown [$^{hydro}(Ca^{2+} + Mg^{2+})$] can be calculated by subtracting twice the value of the $^{cru}SO_4^{2-}$ mass from the total crustal Ca^{2+} and Mg^{2+} mass. Based on (8), the actual numerical value of atmospheric CO_2 drawdown [$^{car\text{-}hydro}CO_2$] during the carbonate hydrolytic process can be obtained using

$$^{car\text{-}hydro}CO_2 = {}^{cru}\left(Ca^{2+} + Mg^{2+}\right) - 2\,{}^{cru}SO_4^{2-} \quad (12)$$

In nature, K/Na-feldspar takes the form of an unstable mineral substance, and atmospheric CO_2, which may be soluble in water, could yield H^+ to accelerate the hydrolysis of K/Na-feldspar [11, 54]. Hence, according to (5) and (6), the amount of atmospheric CO_2 drawdown during K/Na-feldspar hydrolysis should equal the sum of the crustal Na^+ and K^+ contents:

$$^{K/Na}CO_2 = {}^{cru}\left(K^+ + Na^+\right) \quad (13)$$

Figure 6 shows that the total atmospheric CO_2 drawdown for the Koxkar basin during the melting season of 2011 was about 70.98 ± 5.30 kg·C·(km^2·d)$^{-1}$ (i.e., $8.05 \pm 0.60 \times 10^5$ kg C, yield HCO_3^- was ~98.40 ± 7.35 kg·(km^2·d)$^{-1}$). This was well below the 336.34 kg·C·(km^2·d)$^{-1}$ for the Scottbreen basin (3397 kg·C·km^{-2} from 8 July to 5 September 2002) on Svalbard [4] but greater than the fluxes of CO_2 sinks in the Rhône and Oberaar catchments [7] and far more than that in nonglacierized zones [10, 13, 55]. This implies that variation in glacial melting, particularly within the context of climate change, is an important factor in the global CO_2 cycle [56–58].

Globally, runoff HCO_3^- originates from precipitation, ice meltwater, carbonate hydrolysis, and transient drawdown of atmospheric CO_2. The different sources of HCO_3^- were calculated through a detailed analysis of the transient drawdown of CO_2 [4, 11, 52]. Figure 6 shows the HCO_3^- obtained for the Koxkar basin in the above analysis. It can be seen that HCO_3^- was mainly (39.61%) supplied by transient drawdown of CO_2. The secondary source (36.39%) was carbonate hydrolysis, in accordance with the abundance of Paleozoicmarine terrigenous clastic rocks, carbonatite, and Quaternary moraine debris in the Koxkar basin. Only small quantities of HCO_3^- were supplied by ice meltwater and precipitation (20.09% and 3.90%, resp.).

5.4. Revising Hydrochemical Erosion. The transient drawdown of atmospheric CO_2 is an important source of HCO_3^- in the river water of the Koxkar basin. Therefore, the assessment of HCO_3^- from crustal chemical erosion needs to be revised. Crustal HCO_3^- chemical erosion should equal the results obtained in Section 5.2.2 (166.94 ± 9.31 kg·(km^2·d)$^{-1}$) minus the HCO_3^- flux that originated from the transient drawdown CO_2 (~98.40 ± 7.35 kg·(km^2·d)$^{-1}$). Ultimately, the total crustal solute fluxes for hydrochemical erosion should

be about 213.65 ± 10.05 kg·(km^2·d)$^{-1}$ during the sampling period.

6. Conclusions

The CDRs and transient CO_2 drawdown during the melting season of 2011 in a highly glacierized basin at the heart of the Eurasian continent were investigated and the following conclusions drawn:

(1) Streamflow was dominated by glacial ice meltwater, which accounted for 76.49 ± 4.58% of the total discharge in the Koxkar basin. The secondary contributors were groundwater and precipitation, which accounted for 13.71 ± 3.06% and 9.79 ± 1.64%, respectively, from 27 June to 30 September 2011.

(2) CO_2 flux from chemical erosion was 70.98 ± 5.30 kg·C·(km^2·d)$^{-1}$ during the sampling period, which was significantly higher than that in other glacierized regions and nonglacierized regions.

(3) The CDR during the sampling period, derived from the crustal solute flux, was 213.65 ± 10.05 kg·(km^2·d)$^{-1}$, which accounted for 53.59% of the total solute flux of the river water. The solute flux yielded by transient drawdown of CO_2 was 98.40 ± 7.35 kg·(km^2·d)$^{-1}$, which accounted for 24.68% of the total solute of the river water. The solute fluxes from ice meltwater and precipitation were lower: about 70.02 ± 4.68 kg·(km^2·d)$^{-1}$ and 16.57 ± 1.13 kg·(km^2·d)$^{-1}$, respectively, which accounted for 17.57% and 4.16% of the total solute flux.

Conflict of Interests

The authors declare that there is no conflict of interests regarding the publication of this paper.

Acknowledgments

This study was funded by the National Basic Research Program of China (no. 2013CBA01808) and the National Natural Science Foundation of China (nos. 41471060, 4130638, 41271078, and 41201025). The authors appreciate the comments of anonymous reviewers.

References

[1] J. W. Ren, "Updating assessment results of global cryospheric change from SPM of IPCC WGI Fifth Assessment Report," *Journal of Glaciology and Geocryology*, vol. 35, no. 5, pp. 1065–1067, 2013.

[2] Y. J. Ding, S. Y. Liu, J. Li, and D. H. Shangguan, "The retreat of glaciers in response to recent climate warming in western China," *Annals of Glaciology*, vol. 43, pp. 97–105, 2006.

[3] S. Y. Liu, Y. J. Ding, Y. Zhang et al., "Impact of the glacial change on water resources in the Tarim River Basin," *Acta Geographica Sinica*, vol. 61, no. 5, pp. 482–490, 2006.

[4] W. E. Krawczyk and S. A. Bartoszewski, "Crustal solute fluxes and transient carbon dioxide drawdown in the Scottbreen Basin, Svalbard in 2002," *Journal of Hydrology*, vol. 362, no. 3-4, pp. 206–219, 2008.

[5] G. H. Brown, "Glacier meltwater hydrochemistry," *Applied Geochemistry*, vol. 17, no. 7, pp. 855–883, 2002.

[6] G. Dongarrà, E. Manno, G. Sabatino, and D. Varrica, "Geochemical characteristics of waters in mineralised area of Peloritani Mountains (Sicily, Italy)," *Applied Geochemistry*, vol. 24, no. 5, pp. 900–914, 2009.

[7] R. Hosein, K. Arn, P. Steinmann, T. Adatte, and K. B. Föllmi, "Carbonate and silicate weathering in two presently glaciated, crystalline catchments in the Swiss Alps," *Geochimica et Cosmochimica Acta*, vol. 68, no. 5, pp. 1021–1033, 2004.

[8] T. D. L. Irvine-Fynn and A. J. Hodson, "Biogeochemistry and dissolved oxygen dynamics at a subglacial upwelling, Midtre Lovénbreen, Svalbard," *Annals of Glaciology*, vol. 51, no. 56, pp. 41–46, 2010.

[9] J. C. Yde, N. T. Knudsen, and O. B. Nielsen, "Glacier hydrochemistry, solute provenance, and chemical denudation at a surge-type glacier in Kuannersuit Kuussuat, Disko Island, West Greenland," *Journal of Hydrology*, vol. 300, no. 1–4, pp. 172–187, 2005.

[10] P. K. Jha, J. Tiwari, U. K. Singh, M. Kumar, and V. Subramanian, "Chemical weathering and associated CO_2 consumption in the Godavari river basin, India," *Chemical Geology*, vol. 264, no. 1–4, pp. 364–374, 2009.

[11] V. B. Singh, A. L. Ramanathan, J. G. Pottakkal, and M. Kumar, "Seasonal variation of the solute and suspended sediment load in Gangotri glacier meltwater, central Himalaya, India," *Journal of Asian Earth Sciences*, vol. 79, pp. 224–234, 2014.

[12] K. Kumar, M. S. Miral, S. Joshi, N. Pant, V. Joshi, and L. M. Joshi, "Solute dynamics of meltwater of Gangotri glacier, Garhwal Himalaya, India," *Environmental Geology*, vol. 58, no. 6, pp. 1151–1159, 2009.

[13] D. Wolff-Boenisch, E. J. Gabet, D. W. Burbank, H. Langner, and J. Putkonen, "Spatial variations in chemical weathering and CO_2 consumption in Nepalese High Himalayan catchments during the monsoon season," *Geochimica et Cosmochimica Acta*, vol. 73, no. 11, pp. 3148–3170, 2009.

[14] H. D. Han, S. Y. Liu, Y. J. Ding et al., "Near-surface meteorological characteristics on the Koxkar Baxi Glacier, Tianshan," *Journal of Glaciology and Geocryology*, vol. 30, no. 6, pp. 967–975, 2008.

[15] E. S. Kang, S. S. Zhu, and M. M. Huang, "The characteristics of glacier hydrology in the Tumuer region. Glacier and Meteorology in Mt. Tumuer Region, Tianshan," *Urumqi: People's Publishing House of Xinjiang*, pp. 99–119, 1985.

[16] Scientific Expedition Team on Mountaineering of the Chinese Academy of Sciences, *Geology and Paleontology in Tumur Peak Region, Tianshan Mountains*, Xinjiang People's Publishing House, Ürümqi, China, 1985.

[17] H. D. Han, J. Wang, J. F. Wei, and S. Liu, "Backwasting rate on debris-covered Koxkar glacier, Tuomuer mountain, China," *Journal of Glaciology*, vol. 56, no. 196, pp. 287–296, 2010.

[18] E. L. Williams, K. J. Szramek, L. X. Jin, T. C. W. Ku, and L. M. Walter, "The carbonate system geochemistry of shallow groundwater-surface water systems in temperate glaciated watersheds (Michigan, USA): significance of open-system dolomite weathering," *Bulletin of the Geological Society of America*, vol. 119, no. 5-6, pp. 515–528, 2007.

[19] B. G. Mark, J. M. McKenzie, and J. Gómez, "Hydrochemical evaluation of changing glacier meltwater contribution to stream

discharge: Callejon de Huaylas, Peru," *Hydrological Sciences Journal*, vol. 50, no. 6, pp. 975–988, 2005.

[20] J. Wang, Y.-J. Ding, J.-L. Xu, and H.-D. Han, "Hydrochemical characteristic analysis of melting water flow in Keqikaer Glacier, Tianshan (west) Mountains," *Environmental Science*, vol. 27, no. 7, pp. 1305–1311, 2006.

[21] C. L. Li, S. G. Hou, and D. H. Qin, "Spatial differences of hydrochemical and its control factors of the headwater runoff in the Ürümuqi River, Tianshan Mountains," *Journal of Glaciology and Geocryology*, vol. 25, no. 1, pp. 72–76, 2003.

[22] H. B. Zhao, T. D. Yao, and B. Q. Xu, "Hydrological and hydrochemical features of fartamak glacier area in Muztag Ata," *Journal of Glaciology and Geocryology*, vol. 28, no. 1, pp. 269–275, 2006.

[23] S. G. Hou, "Chemical characteristics of precipitation at the headwaters of the Urümuqi River in the Tianshan Mountains," *Journal of Glaciology and Geocryology*, vol. 23, no. 1, pp. 80–84, 2001.

[24] K. Yalcin, C. P. Wake, J. E. Dibb, and S. I. Whitlow, "Relationships between aerosol and snow chemistry at King Col, Mt. Logan Massif, Yukon, Canada," *Atmospheric Environment*, vol. 40, no. 37, pp. 7152–7163, 2006.

[25] X. Li, Z. Li, Y. Ding et al., "Seasonal variations of pH and electrical conductivity in a snow-firn pack on Glacier No. 1, eastern Tianshan, China," *Cold Regions Science and Technology*, vol. 48, no. 1, pp. 55–63, 2007.

[26] L. Krnavek, W. R. Simpson, D. Carlson, F. Domine, T. A. Douglas, and M. Sturm, "The chemical composition of surface snow in the Arctic: examining marine, terrestrial, and atmospheric influences," *Atmospheric Environment*, vol. 50, pp. 349–359, 2012.

[27] R. S. Hindshaw, E. T. Tipper, B. C. Reynolds et al., "Hydrological control of stream water chemistry in a glacial catchment (Damma Glacier, Switzerland)," *Chemical Geology*, vol. 285, no. 1–4, pp. 215–230, 2011.

[28] S. Y. Yang, H. S. Jung, D. I. Lim, and S. Y. Yang, "A review on the provenance discrimination of sediments in the Yellow Sea," *Earth-Science Reviews*, vol. 63, no. 1-2, pp. 93–120, 2003.

[29] D. N. Collins, "Hydrology of an alpine glacier as indicated by the chemical composition of meltwater," *Zeitschrift für Gletscherkunde und Glazialgeologie*, vol. 13, pp. 219–238, 1978.

[30] D. N. Collins, "Quantitative determination of the subglacial hydrology of two Alpine glaciers," *Journal of Glaciology*, vol. 22, no. 89, pp. 347–362, 1979.

[31] M. Tranter and R. Raiswell, "The composition of the englacial and subglacial component in bulk meltwaters draining the Gornergletscher, Switzerland," *Journal of Glaciology*, vol. 37, no. 125, pp. 59–66, 1991.

[32] M. Tranter, G. Brown, R. Raiswell, M. Sharp, and A. Gurnell, "A conceptual model of solute acquisition by Alpine glacial meltwaters," *Journal of Glaciology*, vol. 39, no. 133, pp. 573–581, 1993.

[33] G. H. Brown and M. Tranter, "Hydrograph and chemograph separation of bulk meltwaters draining the upper Arolla Glacier, Valais, Switzerland," in *Hydrology in Mountainous Regions I*, H. Lang and A. Musy, Eds., no. 193, pp. 429–437, IAHS Press, 1990.

[34] F. J. Liu, M. Williams, J. Y. Sun et al., "Hydrochemical process and hydrological separation at the headwaters of the Ürümqi River, Tianshan Mountains, China," *Journal of Glaciology and Geocryology*, vol. 21, no. 4, pp. 362–370, 1999.

[35] C. Gazis and X. H. Feng, "A stable isotope study of soil water: evidence for mixing and preferential flow paths," *Geoderma*, vol. 119, no. 1-2, pp. 97–111, 2004.

[36] I. Braud, T. Bariac, J. P. Gaudet, and M. Vauclin, "SiSPAT-Isotope, a coupled heat, water and stable isotope (HDO and $H_2^{18}O$) transport model for bare soil. Part I. Model description and first verifications," *Journal of Hydrology*, vol. 309, no. 1–4, pp. 277–300, 2005.

[37] D. W. Ostendorf, "Hydrograph and chloride pollutograph analysis of Hobbs Brook reservoir subbasin in eastern Massachusetts," *Journal of Hydrology*, vol. 503, pp. 123–134, 2013.

[38] J. L. McCallum, P. G. Cook, D. Berhane, C. Rumpf, and G. A. McMahon, "Quantifying groundwater flows to streams using differential flow gaugings and water chemistry," *Journal of Hydrology*, vol. 416-417, pp. 118–132, 2012.

[39] K. J. Dinsmore, M. F. Billett, K. E. Dyson et al., "Stream water hydrochemistry as an indicator of carbon flow paths in Finnish peatland catchments during a spring snowmelt event," *Science of the Total Environment*, vol. 409, no. 22, pp. 4858–4867, 2011.

[40] Y. Zhang, S. Y. Liu, Y. J. Ding et al., "Preliminary study of mass balance on the Keqicar Baxi Glacier on the south slopes of Tianshan Mountains," *Journal of Glaciology and Geocryology*, vol. 28, no. 4, pp. 477–484, 2006.

[41] Y. X. Fan, *Granide. Geology and Paleontology in Tuomur Peak Region, Tianshan Mountains*, Xinjiang People's Publishing House, Urümqi, China, 1985.

[42] T. G. Churikova, B. N. Gordeychik, B. V. Ivanov, and G. Wörner, "Relationship between Kamen Volcano and the Klyuchevskaya group of volcanoes (Kamchatka)," *Journal of Volcanology and Geothermal Research*, vol. 263, pp. 3–21, 2013.

[43] I. González-Álvarez and R. Kerrich, "Trace element mobility in dolomitic argillites of the Mesoproterozoic Belt-Purcell Supergroup, Western North America," *Geochimica et Cosmochimica Acta*, vol. 75, no. 7, pp. 1733–1756, 2011.

[44] C. Cordier, L. Folco, and S. Taylor, "Vestoid cosmic spherules from the South Pole Water Well and Transantarctic Mountains (Antarctica): a major and trace element study," *Geochimica et Cosmochimica Acta*, vol. 75, no. 5, pp. 1199–1215, 2011.

[45] J. N. Galloway, Z. Dianwu, X. Jiling, and G. E. Likens, "Acid rain: China, United States, and a remote area," *Science*, vol. 236, no. 4808, pp. 1559–1562, 1987.

[46] B. Bookhagen and M. R. Strecker, "Spatiotemporal trends in erosion rates across a pronounced rainfall gradient: examples from the southern central Andes," *Earth and Planetary Science Letters*, vol. 327-328, pp. 97–110, 2012.

[47] A. R. Stumpf, M. E. E. Madden, G. S. Soreghan, B. L. Hall, L. J. Keiser, and K. R. Marra, "Glacier meltwater stream chemistry in Wright and Taylor Valleys, Antarctica: significant roles of drift, dust and biological processes in chemical weathering in a polar climate," *Chemical Geology*, vol. 322-323, pp. 79–90, 2012.

[48] B. Delmonte, C. Baroni, P. S. Andersson et al., "Modern and Holocene aeolian dust variability from Talos Dome (Northern Victoria Land) to the interior of the Antarctic ice sheet," *Quaternary Science Reviews*, vol. 64, pp. 76–89, 2013.

[49] A. Hodson, P. Porter, A. Lowe, and P. Mumford, "Chemical denudation and silicate weathering in Himalayan glacier basins: Batura Glacier, Pakistan," *Journal of Hydrology*, vol. 262, no. 1–4, pp. 193–208, 2002.

[50] K. L. Ferrier and J. W. Kirchner, "Effects of physical erosion on chemical denudation rates: a numerical modeling study of soil-mantled hillslopes," *Earth and Planetary Science Letters*, vol. 272, no. 3-4, pp. 591–599, 2008.

[51] P. Louvat and C. J. Allègre, "Present denudation rates on the island of réunion determined by river geochemistry: basalt weathering and mass budget between chemical and mechanical erosions," *Geochimica et Cosmochimica Acta*, vol. 61, no. 17, pp. 3645–3669, 1997.

[52] D. P. Dethier and E. D. Lazarus, "Geomorphic inferences from regolith thickness, chemical denudation and CRN erosion rates near the glacial limit, Boulder Creek catchment and vicinity, Colorado," *Geomorphology*, vol. 75, no. 3-4, pp. 384–399, 2006.

[53] D. J. Hercod, P. V. Brady, and R. T. Gregory, "Catchment-scale coupling between pyrite oxidation and calcite weathering," *Chemical Geology*, vol. 151, no. 1–4, pp. 259–276, 1998.

[54] J. R. Price, C. R. Hardy, K. S. Tefend, and D. W. Szymanski, "Solute geochemical mass-balances and mineral weathering rates in small watersheds II: biomass nutrient uptake, more equations in more unknowns, and land use/land cover effects," *Applied Geochemistry*, vol. 27, no. 6, pp. 1247–1265, 2012.

[55] J. Gaillardet, B. Dupré, P. Louvat, and C. J. Allègre, "Global silicate weathering and CO_2 consumption rates deduced from the chemistry of large rivers," *Chemical Geology*, vol. 159, no. 1–4, pp. 3–30, 1999.

[56] S. P. Anderson, J. I. Drever, C. D. Frost, and P. Holden, "Chemical weathering in the foreland of a retreating glacier," *Geochimica et Cosmochimica Acta*, vol. 64, no. 7, pp. 1173–1189, 2000.

[57] W. Ludwig, P. Amiotte-Suchet, and J.-L. Probst, "Enhanced chemical weathering of rocks during the last glacial maximum: a sink for atmospheric CO_2?" *Chemical Geology*, vol. 159, no. 1–4, pp. 147–161, 1999.

[58] K. B. Föllmi, R. Hosein, K. Arn, and P. Steinmann, "Weathering and the mobility of phosphorus in the catchments and forefields of the Rhône and Oberaar glaciers, central Switzerland: implications for the global phosphorus cycle on glacial–interglacial timescales," *Geochimica et Cosmochimica Acta*, vol. 73, no. 8, pp. 2252–2282, 2009.